Published in final edited form as:

*Cancer Res*. 2020 March 01; 80(5): 1156–1170. doi:10.1158/0008-5472.CAN-19-1601.

# Host Wnt5a Potentiates Microenvironmental Regulation of Ovarian Cancer Metastasis

**Marwa Asem**[1,2,3], **Allison M. Young**[3], **Carlysa Oyama**[3], **Alejandro Claure De La Zerda**[3], **Yueying Liu**[2,3], **Jing Yang**[2,3], **Tyvette S. Hilliard**[2,3], **Jeffery Johnson**[2,3], **Elizabeth I. Harper**[2,3], **Ian Guldner**[3,4], **Siyuan Zhang**[3,4], **Toni Page-Mayberry**[3], **William J. Kaliney**[3], **M. Sharon Stack**[1,2,3]

[1]Integrated Biomedical Sciences Program, University of Notre Dame, South Bend, Indiana.

[2]Department of Chemistry and Biochemistry, University of Notre Dame, South Bend, Indiana.

[3]Harper Cancer Research Institute, University of Notre Dame, South Bend, Indiana.

[4]Department of Biological Sciences, University of Notre Dame; South Bend, Indiana.

## Abstract

The noncanonical Wnt ligand Wnt5a is found in high concentrations in ascites of women with ovarian cancer. In this study, we elucidated the role of Wnt5a in ovarian cancer metastasis. Wnt5a promoted ovarian tumor cell adhesion to peritoneal mesothelial cells as well as migration and invasion, leading to colonization of peritoneal explants. Host components of the ovarian tumor microenvironment, notably peritoneal mesothelial cells and visceral adipose, secreted Wnt5a. Conditional knockout of host *WNT5A* significantly reduced peritoneal metastatic tumor burden. Tumors formed in *WNT5A* knockout mice had elevated cytotoxic T cells, increased M1 macrophages, and decreased M2 macrophages, indicating that host Wnt5a promotes an immunosuppressive microenvironment. The Src family kinase Fgr was identified as a downstream effector of Wnt5a. These results highlight a previously unreported role for host-expressed Wnt5a

**Corresponding Author:** M. Sharon Stack, University of Notre Dame, 1234 Notre Dame Ave., South Bend, IN 46617. Phone: 574-631-4100; Fax: 574-631-2156; sharon.stack.11@nd.edu.

Authors' Contributions

**Conception and design:** M. Asem, M.S. Stack

**Development of methodology:** M. Asem, Y. Liu, J. Yang, I. Guldner, S. Zhang

**Acquisition of data (provided animals, acquired and managed patients, provided facilities, etc.):** M. Asem, C. Oyama, A. Claure De La Zerda, Y. Liu, J. Yang, T.S. Hilliard, J. Johnson, E.I. Harper, I. Guldner, S. Zhang, T. Page-Mayberry

**Analysis and interpretation of data (e.g., statistical analysis, biostatistics, computational analysis):** M. Asem, C. Oyama, A. Claure De La Zerda, Y. Liu, J. Yang, I. Guldner

**Writing, review, and/or revision of the manuscript:** M. Asem, T.S. Hilliard, I. Guldner, M.S. Stack

**Administrative, technical, or material support (i.e., reporting or organizing data, constructing databases):** M. Asem, A.M. Young, Y. Liu, J. Yang, S. Zhang

**Study supervision:** M. Asem, M.S. Stack

**Other (prepared tissue sample gel through "tissue fixation" for the slides; analyzed slide images for data on cancer cells present across control and experimental specimens):** A.G. Claure De La Zerda

**Other (histologic and IHC interpretation and correlation):** W.J. Kaliney

The costs of publication of this article were defrayed in part by the payment of page charges. This article must therefore be hereby marked *advertisement* in accordance with 18 U.S.C. Section 1734 solely to indicate this fact.

**Note:** Supplementary data for this article are available at Cancer Research Online (http://cancerres.aacrjournals.org/).

Disclosure of Potential Conflicts of Interest

No potential conflicts of interest were disclosed.

in ovarian cancer metastasis and suggest Fgr as a novel target for inhibition of ovarian cancer metastatic progression.

## Significance:

This study establishes host-derived Wnt5a, expressed by peritoneal mesothelial cells and adipocytes, as a primary regulator of ovarian cancer intraperitoneal metastatic dissemination and identifies Fgr kinase as novel target for inhibition of metastasis.

## Introduction

The majority of women diagnosed with ovarian cancer succumb to metastatic disease characterized by diffuse intraperitoneal carcinomatosis (1). Ovarian tumors are genetically highly heterogeneous, exhibiting massive genomic and transcriptomic plasticity; however, no single genetic alteration has yet been found to be a clinically actionable genetic change (2–4). Thus, a more comprehensive understanding of tumor–host interactions in metastasis may highlight novel strategies for therapeutic intervention. Widespread intraperitoneal metastasis results from direct extension or exfoliation of cells from the primary tumor into the peritoneal cavity. Hematogenous metastasis with peritoneal homing has also been reported (5, 6). Metastasizing cells colonize the omental fat pad, the ovary, and peritoneum. Matrix-detached cells survive in a complex ascites fluid phase, yet subsequently adhere to the mesothelial cells of the peritoneal membrane that covers abdominal organs, anchor in the collagen-rich submesothelial matrix, and proliferate to produce hundreds of widely disseminated secondary lesions (6).

Ascites fluid functions as a rich reservoir of soluble and cellular components that influence primary tumor growth, progression, and metastasis (7). We previously found high levels of Wnt5a in ascites fluids of women with ovarian cancer (8). This noncanonical Wnt ligand is of interest because of its role in regulation of cell polarity and morphogenesis and its link to cancer initiation and progression (8). Moreover, conflicting data have been reported on the role of Wnt5a in ovarian cancer progression. In one study, expression of Wnt5a was lower in primary ovarian tumors relative to normal ovarian surface or fallopian tube epithelium. Low Wnt5a expression was correlated with both tumor stage and overall survival, suggesting that loss of Wnt5a is predictive of poor outcome (9). In contrast, several additional studies report that high Wnt5a expression in ovarian cancer tissues correlates with poor prognosis and demonstrate Wnt5a upregulation in platinum-resistant tumors, suggesting a role for Wnt5a in acquired chemoresistance (10–12).

In the current study, we have used a comprehensive suite of *in vitro*, *ex vivo*, and *in vivo* analyses to elucidate the role of Wnt5a in ovarian cancer metastasis. Herein, we demonstrate that Wnt5a is contributed by host cells in the peritoneal microenvironment, specifically peritoneal mesothelial cells and visceral adipose tissue. Conditional knockout of host *WNT5A* significantly reduces tumor burden and alters the immune landscape of peritoneal tumors. The Src family kinase Fgr is identified as a novel downstream effector of Wnt5a in ovarian cancer cells and selective inhibition of Fgr kinase activity abrogates prometastatic cellular activity. Together, our results highlight a previously unreported role for host-

expressed Wnt5a in modulation of ovarian cancer metastatic success in the peritoneal microenvironment.

## Materials and Methods

### Reagents

Recombinant Wnt5a protein (rWnt5a), Proteome Profiler Human Phospho-Kinase Array, and Proteome Profiler mouse cytokine array were purchased from R&D Systems. Rat tail collagen type I was purchased from Corning Cellgro. 4-Hydroxytamoxifen was purchased from Sigma-Aldrich. TL02–59 was purchased from ProbeChem.

### Cell culture

The epithelial ovarian carcinoma cell lines DOV13, OVCA429, and OVCA433 were provided by Dr. Robert Bast (University of Texas MD Anderson Cancer Center, Houston, TX). OVCAR3, OVCAR5, and OVCAR8 cells were obtained from ATCC. OVCAR3 cells were maintained in RPMI1640 medium (Corning Cellgro), containing 10% FBS (Gibco), 1% penicillin/streptomycin (Lonza), and 1% L-GlutaMax (Thermo Fisher Scientific). OVCAR5 and OVCAR8 cells were maintained in DMEM medium, containing 10% FBS, 1% penicillin/streptomycin, and 1% Non-Essential Amino Acids (Gibco). DOV13, OVCA429, and OVCA433 were maintained in minimal essential medium (Gibco) containing 10% FBS, 1% nonessential amino acids (Corning Cellgro), 1% penicillin/streptomycin (Lonza), 1% sodium pyruvate (Corning Cellgro), and 0.1% amphotericin B (Cellgro); DOV13 medium was additionally supplemented with 10 μg/mL of insulin (Gibco). Cell lines were tested and authenticated by Genetica DNA Laboratories using short tandem repeat DNA profiling and were found to be >95% concordant. Cells tested negative for *Mycoplasma* in 2017. The C57Bl/6 syngeneic mouse ovarian cancer cell line (ID8) with a CRISPR/Cas9–generated *TRP53* gene deletion (designated ID8-Trp53$^{-/-}$), generously provided by Dr. I. McNeish, Glasgow, United Kingdom, was tagged with red fluorescent protein (RFP) and maintained as described previously (13, 14). Primary human peritoneal mesothelial cells (Zen-Bio) and the normal human peritoneal mesothelial cell line LP9 (Coriell Institute, Camden, NJ) were maintained in Medium 199, Ham 12 medium, containing 15% FBS, 10 ng/mL EGF, 400 ng/mL hydrocortisone, 1% penicillin/streptomycin, 1% L-GlutaMax (Thermo Fisher Scientific), and 1% HEPES. Murine primary peritoneal mesothelial cells (MPMC) were isolated from 4- to 6-month-old C57Bl/6 J mice as described previously (15). Primary mesothelial cells were grown in modified Connell's Medium composed of DMEM/F12 þ GlutaMAX (Gibco), 15% FCS, 0.4 μg/mL hydrocortisone, 10 ng/mL EGF, 1% ITS (insulin, transferrin, selenium), 1 mmol/L sodium pyruvate, 0.1 mmol/L β-mercaptoethanol (2-ME), 1% nonessential amino acids, 1% penicillin/streptomycin, and 2% Mycokill (PAA). All cells were maintained at 37°C, 5% $CO_2$ in humid air. To produce conditioned media (CND), cells were grown to approximately 80% to 100% confluence and washed three times with PBS prior to addition of serum free medium for 24 hours.

### Organotypic mesomimetic adhesion assay

Human LP9 peritoneal mesothelial cells were grown on cover slips containing type I collagen gels (10 μg/mL) until confluency. RFP-tagged OVCAR3, OVCAR5, and OVCAR8 cells were serum starved overnight then treated with serum-free media, rWnt5a protein (0.4 μg/mL), LP9-CND, or LP9-Wnt5a$^{KO}$-CND for 24 hours. In some experiments, cells were pretreated with Wnt5a function-blocking antibody (MAB645, R&D Systems) or control IgG at 2 μg/mL for 24 hours prior to use. Cells ($5 \times 10^4$) from each treatment condition then were added atop of the confluent mesomimetic and allowed to adhere for 20 minutes and 1 hour, respectively. Mesomimetic cultures were washed with PBS; adherent cells were imaged with Echo Revolve fluorescent microscope and quantified using ImageJ software. The assay was done in three experimental replicates and repeated in three biological replicates for all conditions.

### *Ex vivo* adhesion assay

To evaluate adhesion to mesothelial cells on intact peritoneal tissue, an *ex vivo* peritoneal explant assay was used (16). An optically clear solid support was prepared using Sylgard 184 Silicone Elastomer Kit (Thermo Fisher Scientific) according to the manufacturer's specifications. Mice were first euthanized by $CO_2$ inhalation followed by cervical dislocation and then rapidly dissected using a ventral midline incision. After skin removal, the parietal peritoneum lining the ventral abdominal wall was dissected to remove a 1.2 × 1.2 $cm^2$ piece of peritoneal tissue immediately adjacent to the midline in the lower two abdominal quadrants. The tissue explant was then pinned mesothelialside up to the silastic resin using fine gauge dissecting pins and the explant immersed in PBS. RFP-OVCAR5 and RFP-OVCAR8 cells were serum starved overnight then treated with serum-free media, rWnt5a protein (0.4 μg/mL), LP9-CND or LP9-Wnt5a$^{KO}$-CND for 24 hours. RFP-OVCAR5 and RFP-OVCAR8 cells ($5 \times 10^4$) from each treatment condition were added to the explant and incubated for 30 and 90 minutes, respectively, at 37°C, were vigorously washed in PBS (five times), and mounted onto a glass coverslip. Adherent cells were imaged with either the Echo Revolve fluorescent microscope or EVOS FL digital inverted fluorescence microscope and cells were counted manually using ImageJ software. The assay was done in three experimental replicates and repeated in three biological replicates for all conditions. Additional explants were processed for scanning electron microscopy as described below.

### Immunofluorescence microscopy

Cells were cultured on 22 $mm^2$ glass coverslips coated with type I collagen (10 μg/mL) and treated with rWnt5a (0.4 μg/mL) for 24 hours. Coverslips were washed twice with ice-cold PBS and fixed with 4% paraformaldehyde in 0.12 mol/L sucrose in PBS for 30 minutes at room temperature. Nonspecific binding was blocked with 5% normal goat serum in PBS for 1 hour at room temperature. Coverslips were then incubated with phalloidin488 (1:100; Thermo Fisher Scientific) in 1% normal goat serum in PBS for 20 minutes in room temperature and rinsed three times for 5 minutes with PBS. After washing, cells were air-dried, mounted with VECTASHIELD Mounting Media with 4′, 6-diamidino-2-phenylindole (DAPI; Vector Laboratories), and imaged with a Leica DM5500 fluorescence microscope (Leica Biosystems, Inc.).

### Scanning electron microscopy

Murine peritoneal explants were dissected from the 4- to 6-month-old C57Bl/6 J mice as described above and processed directly for scanning electron microscopy. Tissues were fixed for scanning electron microscopy (2% glutaraldehyde, 2% paraformaldehyde in 0.1 mol/L cacodylate, pH 7.35, 1 hour), washed using 2-ME buffer (0.1 mol/L sodium cacodylate, pH 7.35, containing 0.13 mol/L sucrose, 0.01 mol/L 2-ME; three times, 20 minutes each), and fixed with osmium tetroxide (2% in cacodylate buffer) with microwave processing. After rinsing with cacodylate buffer and washing with ultrapure water (three times, 5 minutes each), tissues were dehydrated in a graded series of ethanol, subjected to critical point drying, placed on carbon stubs, and sputter-coated with platinum. Samples were examined using a FEI-Magellan 400 Field Emission scanning electron microscope in the Electron Microscopy core of the Notre Dame Integrated Imaging Facility.

### Analysis of migration and invasion

To assess cell migration, cells ($1 \times 10^5$) were seeded atop an 8-μm microporous membrane located within the upper compartment of a transwell insert (BD Biosciences), and incubated at 37°C for 24 hours. After incubation, migrated cells passing through the 8-μm pore filter were fixed, stained with Diff-Quik (Thermo Fisher Scientific), and enumerated using ImageJ software. All experiments were completed in triplicate and five fields/well were counted. To assess invasion, an 8-μm microporous membrane located within the upper compartment of a transwell insert (BD Biosciences) was coated with 20 μg of rat tail type I collagen in sodium carbonate, pH 9.6 overnight at 4°C, washed with PBS, and air dried. Cells were seeded atop the filter and the apparatus incubated at 37°C for 24 hours. After incubation, invaded cells passing through the collagen and 8mm pore filter were fixed, stained with Diff-Quik (Thermo Fisher Scientific), and enumerated using ImageJ software. All experiments were completed in triplicate and five fields/well were counted.

### RNA isolation and qRT-PCR

Total RNA was extracted from cells or tissues using RNeasy Mini Kit (Qiagen) in accordance with the manufacturer's instructions. cDNA was synthesized from 1 to 5 μg of total RNA using $RT^2$ First Strand Kit (Qiagen). Real-time PCR was performed on a StepOnePlus Real-Time PCR System (Applied Biosystems). PCR primers for *WNT5A*, *ROR1/2*, and *FZDs* are described in Supplementary Table S1.

### ELISA

Wnt5a protein concentration was measured in duplicate conditioned media using a commercially available Wnt5a sandwich ELISA Kit according to the manufacturer's protocol (Cloud-Clone Corp.).

### Immunohistochemistry

Mice were sacrificed for dissection following Institutional Animal Care and Use Committee (IACUC) protocol. Organs were collected and fixed in 10% formalin, paraffin embedded, and sectioned (5 μm). Tissue sections were stained and IHC analysis of Wnt5a was performed using rat monoclonal anti-Wnt5a (1:200; Abcam). Human tumor microarray

sections were stained with rabbit polyclonal phospho-Fgr (1:200; Thermo Fisher Scientific). Anti-rat and anti-rabbit IgG and peroxidase detection system reagents (DAB chromogen) were purchased from Abcam, Vector Laboratories, and BioGenex, respectively. Slides were scanned into the eSlide Manager database (version 12.3.2.5030) with the Aperio ScanScope CS (Leica, Biosystems, Inc.).

### Wnt5a shRNA transduction

LP9 cells were transduced with eight different *WNT5A* human shRNA lentiviral particles or control scrambled shRNA lentiviral particles expressing GFP and puromycin (pGFP-C-shLenti), following the manufacturer's protocol (OriGene Technologies, Inc.; Supplementary Table S1). Stable transduced cells were selected by culturing in LP9 medium containing 1.2 μg/mL puromycin for 10 days. Stably transduced cells were passaged in culture for preparation for functional assays. The GFP expressed in the lentiviral vectors was used to measure transduction efficiency and qPCR and ELISA were used to select the transduced cells with the highest knockdown efficiency.

### Generation of mice with conditional *WNT5A* knockout

C57BL/6J mice with whole-body, inducible knockout of *WNT5A* ($Wnt5a^{KO}$, tamoxifen) were generated by crossing *WNT5A* floxed mice ($Wnt5a^{fl/fl}$) with UBC-Cre/ERT2 mice (The Jackson Laboratory). In the offspring ($Wnt5a^{fl/fl}$/UBC-$Cre^{+/-}$ mice), *WNT5A* exon2 was deleted by administering 4-hydroxytamoxifen (Sigma-Aldrich) daily to 6-week-old mice for 7 consecutive days to induce the activation of the Cre-ERT2 recombinase and remove the floxed *WNT5A* coding gene (17). Vehicle-treated $Wnt5a^{fl/fl}$/UBC-$Cre^{+/-}$ ($Wnt5a^{fl/fl}$/UBC-$Cre^{+/-}$, vehicle) mice or tamoxifen-treated $Wnt5a^{fl/fl}$ mice ($Wnt5a^{fl/fl}$, tamoxifen) were used as controls in tumor allograft studies. Mice were genotyped by PCR with the recommended primer pairs from The Jackson Laboratory (Supplementary Table S2). Normal C57BL/6J mice were included in the study as an imaging control. All mice were housed in the Association for Assessment and Accreditation of Laboratory Animal Care–approved Freimann Life Sciences Center vivarium and experiments were approved by the Institutional Animal Care and Use Committee at the University of Notre Dame (South Bend, IN).

### Murine allograft model of ovarian cancer metastasis

As ovarian cancer cells disseminate directly from the primary tumor into the peritoneal cavity, syngeneic murine ovarian cancer cells (ID8-$Trp53^{3-/-}$, $5 \times 10^6$ cells) were injected intraperitoneally into $Wnt5a^{KO}$, tamoxifen mice and control mice to assess intraperitoneal metastatic dissemination. To monitor tumor progression, live mice were longitudinally imaged once a week beginning at 3 weeks postinjection under isoflurane anesthesia, using the Bruker Xtreme In Vivo Imaging system. During the study, mice were observed for signs of lethargy or ascites accumulation. Mice were sacrificed at 5 weeks postinjection following University of Notre Dame IACUC-approved protocols. Ascites and peritoneal lavage were collected after intraperitoneal injection of 2 mL PBS. The abdominal cavity was imaged then the abdominal organs were collected, and imaged *ex vivo* as previously described using the Bruker Xtreme In Vivo Imaging system (18). Abdominal tumor burden and organ-specific tumor burden were quantified using ImageJ as described previously (18). After imaging,

organs were fixed in 10% formalin and processed for paraffin embedding for histologic analysis.

### Peritoneal immune profiling by mass cytometry (CyTOF)

Simultaneous interrogation of multiple immune cell types in peritoneal lavage fluid was performed using a CyTOF2 Mass Cytometry System (Fluidigm Corporation) in the Flow Cytometry Resource Facility of the Indiana University Simon Cancer Center. Peritoneal lavage was collected from tumor-free mice by injecting Wnt5A knockout or control mice intraperitoneally with 5 mL cold RPMI media and retrieval of the lavage fluid. Red blood cells were lysed with RBC Lysis Buffer (BioLegend, 420301). Cells were washed and resuspended in Maxpar PBS (Fluidigm, 201058). Dead cells were labeled by incubation with Cell-ID Cisplatin (0.75 μmol/L, Fluidigm, 201064) for 5 minutes and then washed in Maxpar Cell Staining Buffer (Fluidigm, 201068). FC receptors were blocked by incubation with TruStain fcX in MaxPar Cell Staining Buffer (100 μL) for 30 minutes at room temperature. Cells were washed and then stained with a cocktail of metal-conjugated antibodies as indicated below at room temperature for 30 minutes and then washed in MaxPar Cell Staining Buffer. Optimal concentrations were determined for each antibody by titration. The following preconjugated antibodies purchased from Fluidigm were used in this study: CD45–089Y (3089005B, 30-F11); Ly-6G-141Pr (3141008B, 1A8,); CD11c-142Nd (3142003B, N418); CD45R-144Nd (3144011B, RA3–6B2); CD4–145Nd (3145002B, RM4–5); CD11b-148Nd (3148003B, M1/70); CD44–150Nd (3150018B, IM7); CD25–151Eu (3151007B, 3C7); CD3e-152Sm (3152004B, 145–2C11); PD-L1–153Eu (3153016B, 10F.9G2); CTLA-4–154Sm (3154008B, UC10–4B9); PD-1–159Tb (3159024B, 29F.1A12); Ly-6C-162Dy (3162014B, HK1.4); CX3CR1–164Dy (3164023B, SA011F11); NK1.1–165Ho (3165018B, PK136); ckit-166Er (3166004B, 2B8); CD8a-168Er (3168003B, 53–6.7); CD86–172Yb (3172016B, GL1); I-A/I-E-209Bi (3209006B, M5/114.15.2). Cells were resuspended and fixed in 1.6% PFA prepared in MaxPar PBS for 20 minutes and then washed in MaxPar PBS. Nuclei were labeled by incubating fixed cells in Cell-ID Intercalator (1:4,000, Fluidigm, 201192B) dissolved in MaxPar Fix and Perm Buffer (Fluidigm, 201067) for 1 hour or overnight at 4°C. Following nuclear labeling, cells were washed once in MaxPar Cell Staining Buffer and twice in MaxPar Water (Fluidigm, 201069). Samples were brought to 500,000 particulates/mL in MilliQ water containing 0.1× EQ beads (Fluidigm, 201078) and run in 450 μL injections on the CyTOF2 instrument.

### Proteome profiler mouse cytokine array

The Proteome Profiler Mouse Cytokine Array Kit (Panel A; R&D Systems) was used to profile cytokines in 200 μL of ascites or peritoneal lavage samples according to the manufacturer's protocol. The array membranes were imaged with ImageQuant LAS 4000 biomolecular imager (GE Healthcare). Densitometry analysis was carried out using ImageJ.

### Immunofluorescence analysis of murine tissue specimens

Murine peritoneal organs were collected as described above, fixed in 10% formalin, paraffin embedded, and cryosectioned (6 μm). Tissue sections were stained with rabbit polycolonal CD8 (1:200; Biorbyt), mouse monoclonal FOXP3 (1:1,600; Abcam), rabbit polycolonal CD206 (1:30,000; Abcam), rabbit polyclonal iNOS (1:2,000; Abcam), and rat monoclonal

F4/80 (1:50; Abcam) at 4C overnight and the entire tumor section was evaluated for tumor infiltrating T cells using a Leica DM5500 fluorescence microscope with 25× objective lens. Whole tumor areas were scanned and T cells were counted manually per each whole tumor area. The average of $CD8^+$ or $FOXP3^+$ cells for three mice per cohort was used for statistical analysis. For macrophage quantification, 10 independent areas with the most abundant macrophages per mouse were selected and imaged with a 25× objective lens. The area percentage covered by $F4/80^+$ $iNOS^+$ or $F4/80^+$ $CD206^+$ were calculated per each image using ImageJ.

### Proteome profiler human phosphokinase array

Human phosphokinase antibody array purchased from R&D Systems was used to detect the expression of 43 kinase phosphorylation sites on proteins isolated from OVCAR5 and OVCAR8 cells treated with SFM or 0.4 μg/mL rWnt5a for 24 hours. Cell lysates were incubated with antibody array membranes in a multi-well dish overnight and signal detected by chemiluminescence according to the manufacturer's protocol using ImageQuant LAS 4000 biomolecular imager (GE Healthcare). Capture and control antibodies are spotted in duplicate on nitrocellulose membranes. Densitometric analysis was carried out using ImageJ.

### Western blotting

Cells were serum starved for 2 hours or overnight then incubated in SFM ±TL02–59 (0.01 or 1.0 μmol/L) or rWnt5a (0.4 μg/mL) for varying time points. Cells were then lysed and collected using mRIPA lysis buffer (1% Triton X-100, 50 mmol/L Tris, pH 7.5, 150 mmol/L NaCl, 5 mmol/L EDTA, 0.1% SDS, 20 mmol/L NaF, 10 mmol/L $Na_2P_2O_7$) supplemented with protease inhibitor mixture (Roche Applied Science), and protein concentration was determined using the Bio-Rad DC Protein Assay Kit. Cell lysates (20 μg) were electrophoresed on 12% SDS-polyacrylamide gels, transferred to Immobilon-P PVDF membrane (EMD Millipore) using a Trans-Blot S.D. semi-dry transfer cell (Bio-Rad), and blocked with 3% BSA in TBST buffer (20 mmol/L Tris, pH 7.5, 150 mmol/L NaCl, 0.1% Tween 20) for 1 hour at room temperature. Membranes were incubated overnight at 4°C with the primary antibodies listed below. The immunoreactive proteins were visualized with horseradish peroxidase-conjugated goat anti-rabbit IgG or anti-mouse IgG (1:4,000; Sigma-Aldrich) followed by enhanced chemiluminescent developing with SuperSignal West Dura extended duration substrate (Thermo Fisher Scientific) using an ImageQuant LAS 4000 biomolecular imager (GE Healthcare). Protein blots were then stripped and reblotted with anti-β-actin-peroxidase antibody (A3854, clone AC-15, 1:100,000; Sigma-Aldrich) to ensure that similar amounts of protein were present in each lane. Protein band intensities were quantified by densitometric analysis using ImageJ software, and values were normalized to β-actin loading control and expressed as a ratio. The assay was repeated at least in three independent biological replicates. The primary antibodies used for Western blotting are rabbit polyclonal phospho-Fgr (1:1,000; Thermo Fisher Scientific), mouse monoclonal c-Fgr (1:1,000; Santa Cruz Biotechnology).

### Statistical analysis

All experiments were repeated for at least three times independently as indicated. The statistical analysis of the data was done using GraphPad Prism software or Excel software. Data are (where indicated) presented as mean ± SD or SEM. Comparison between groups was performed using Student two-tailed *t* test to determine *P* values. $P < 0.05$ was considered statistically significant.

## Results

### Wnt5a potentiates ovarian cancer cell prometastatic behavior

Metastasis to the peritoneum is present in >80% of patients with ovarian cancer (16). The peritoneum is a vast serous membrane that lines the inner walls of the abdominal cavity and the outside of the visceral organs with a continuous surface area of 1 to 2 $m^2$, nearly equivalent to that of the skin (19). The peritoneum is comprised of a monolayer of mesothelial cells (MC), which lie atop a submesothelial matrix mainly consisting of type I collagen with scattered fibroblasts and immune cells (20). Metastatic cells are shed from the primary tumor into the peritoneal cavity, leading to the buildup of ascites that facilitates intraperitoneal and retroperitoneal metastasis and correlates with reduced survival. As we previously reported that Wnt5a is highly abundant in ovarian cancer ascites fluid (0.4 μg/mL; ref. 8), we investigated the effect of Wnt5a on ovarian cancer cell behavior using the human ovarian cancer cell lines OVCAR5 and OVCAR8, selected on the basis of low endogenous *WNT5A* mRNA and Wnt5a protein levels and the expression of Wnt5a-binding receptors (Supplementary Fig. S1A–S1C). Our initial experiments used 3-dimensional organotypic mesomimetic cultures, comprised of human peritoneal mesothelial cells on collagen gels, to evaluate early adhesive events in metastasis (21). OVCAR5 and OVCAR8 cells treated with recombinant Wnt5a (rWnt5a) at levels found in human ovarian cancer ascites (0.4 μg/mL) showed a 3- to 4-fold increase in adhesion to mesomimetic cultures relative to controls (Fig. 1A–C; ref. 22). On the basis of these data, we then examined ovarian cancer cell interaction with murine peritoneal explants maintained *ex vivo* (14). Consistent with the mesomimetic adhesion assay, rWnt5a treatment enhanced adhesion to intact murine peritoneal explants by 12- to 15-fold (Fig. 1D–F). Furthermore, in both ovarian cancer cell lines, migration and invasion of type I collagen gels was enhanced 6- to 10-fold and 3- to 4-fold, respectively, by rWnt5a treatment (Fig. 1G–J). Consistent with these findings are striking alterations in ovarian cancer cell morphology, with enhanced elaboration of filopodia and lamellapodia known to potentiate cell motility and invasion (Fig. 1K–L). Given these data, we reasoned that Wnt5a may be a potential driver of ovarian cancer cell aggressiveness in the peritoneal cavity by inducing prometastatic behaviors including OvCa:MC adhesion as well as ovarian cancer cell migration and invasion.

### Host peritoneal cells contribute Wnt5a to the ovarian cancer tumor microenvironment

As ascites fluid, rich in soluble Wnt5a, receives contributions from both tumor and host components, we examined the expression of *WNT5A* mRNA and Wnt5a protein by two major cellular components of the peritoneal microenvironment; peritoneal MC and visceral adipose tissues including the omentum and periovarian and uterine fat pads (23). For comparison to human samples, we used OVCAR3 cells, selected because they express the

highest levels of *WNT5A* mRNA and Wnt5a protein (Supplementary Fig. S1). Primary peritoneal MCs derived from either human or murine sources (HPMCs and MPMCs, respectively) as well as the human peritoneal MC cell line LP9 express substantially higher levels of *WNT5A* mRNA relative to syngeneic OVCAR3 (human) and ID8-Trp53$^{-/-}$ (murine) tumor cells (Fig. 2A and B), and Wnt5a protein levels were 3- to 5-fold higher in HPMC and LP9 conditioned medium relative to OVCAR3 (Fig. 2C). Moreover, high level *WNT5A* expression was also observed in murine visceral adipose depots compared to murine ID8-Trp53$^{-/-}$ ovarian cancer cells (Fig. 2D; refs. 17, 24), and this was confirmed by IHC analysis (Fig. 2E).

## Silencing of *WNT5A* from peritoneal MCs modulates ovarian cancer prometastatic behavior

Given the potential contribution of peritoneal MC-derived Wnt5a to prometastatic behaviors that predict ovarian cancer metastatic success, we next sought to examine the functional consequences of silencing *WNT5A* expression in the human peritoneal MC line LP9. Human LP9 cells deficient in Wnt5a (LP9-Wnt5a$^{KD}$) were generated (Supplementary Fig. S2A–S2C), and conditioned media were collected from parental LP9 cells (LP9-CND) or LP9-Wnt5a$^{KD}$ cells (LP9-Wnt5a$^{KD}$-CND). Silencing of *WNT5A* expression significantly impaired OVCAR5 and OVCAR8 cell adhesion to MCs in both organotypic meso-mimetic assays (Supplementary Fig. S2D and Fig. 2F) and to intact murine peritoneal explants in *ex vivo* adhesion assays (Supplementary Fig. S2E and Fig. 2G). Cell motility, but not collagen invasion, was also impaired (Supplementary Fig. S2F and S2G; Fig. 2H and I), suggesting the presence of additional factors produced by LP9 cells, independent of Wnt5a, that promote collagen invasion. Moreover, neutralizing of Wnt5a produced by OVCAR3 cells significantly reduced adhesion to mesomimetic cultures (Supplementary Fig. 2H). Overall, these data strongly support a role for host peritoneal MC-derived Wnt5a in promoting prometastatic behavior in ovarian cancer cells.

## Conditional whole-body silencing of host *WNT5A* expression confirms role of host-derived Wnt5a in ovarian cancer metastatic progression

Supported by these data, we next designed an approach to examine the influence of host-derived Wnt5a on ovarian cancer metastatic success *in vivo*. Considering that Wnt5a expression is critical for normal embryogenesis and that conventional *WNT5A*-nullizygous mice exhibit perinatal lethality, we generated an inducible whole-body *WNT5A* knockout transgenic mouse model by crossing *WNT5A*$^{fl/fl}$ mice with mice expressing a tamoxifen-inducible Cre/ERT2 recombinase that is expressed in all mouse tissues under the control of ubiquitin C promoter (UBC-Cre$^{+/-}$) to generate whole-body Wnt5a knockout mice (Wnt5a$^{KO}$, tamoxifen; (Fig. 3A; Supplementary Fig. S3A; ref. 17). These mice, together with a panel of controls, were then used in syngeneic allograft studies to evaluate whether loss of host-derived Wnt5a alters metastatic progression. Controls included vehicle-injected Wnt5a$^{fl/fl}$, UBC$^{Cre+/-}$mice (Wnt5a$^{fl/fl}$, UBC$^{Cre+/-}$, vehicle) and tamoxifen-injected Wnt5a$^{fl/fl}$ (Wnt5a$^{fl/fl}$, tamoxifen) mice as well as normal mice as imaging controls (Fig. 3A and B). Syngeneic murine RFP-tagged ID8-Trp53$^{-/-}$ cells were injected intraperitoneally and mice were imaged longitudinally to monitor tumor progression (Supplementary Fig. S3B). At 5 weeks postinjection, mice in all cohorts were sacrificed, the abdominal cavity

was exposed for *in situ* imaging (Fig. 3C), and abdominal tumor area and the abdominal tumor intensity were quantified (Fig. 3D and E; ref. 18). Mice deficient in Wnt5a expression ($Wnt5a^{KO}$, tamoxifen) had a 3- to 11-fold reduction in overall peritoneal tumor burden relative to controls (Fig.3D and E). Moreover, *ex vivo* imaging of individual organs showed a significant reduction in organ-specific tumor burden (Fig. 3F and G) and ascites formation (Fig. 3H) in *WNT5A* knockouts relative to controls, supporting the hypothesis that host peritoneal Wnt5a contributes significantly to ovarian cancer metastatic progression.

## Wnt5a modulates immune infiltrates in ovarian metastases

Given that Wnt5a has been shown to regulate immune cell chemotaxis and cytokine secretion (8, 25–28), we next sought to discern whether loss of *WNT5A* expression altered the peritoneal immune landscape. We investigated cytokine profiles in peritoneal lavage fluids in control experiments using a proteome profiler mouse cytokine array. Under basal conditions in disease-free mice, no differences in cytokine profiles were observed (Supplementary Fig. S3C). We then used mass cytometry (CyTOF) to profile and quantify peritoneal immune cells in disease-free mice using a panel of 19 immune cell and immune functionality markers (Fig. 4A). We identified a rich diversity of immune cells consisting of both innate and adaptive immune cells; however, differences in immune cell frequencies were not statistically significant (Fig. 4B). We also examined PD-1 and CTLA-4 expression among T-cell subsets. CTLA-4 was not appreciably expressed on T cells of control or knockout animals and PD-1 expression on $CD4^+$ and $CD8^+$ T cells was not significantly different between groups. Together, these data indicate that the peritoneal immune microenvironments of control and *WNT5A* knockout mice are not appreciably different prior to tumor initiation.

In contrast to results observed in disease-free mice, in tumor-bearing animals, cytokine array data showed that $Wnt5a^{KO}$, tamoxifen mice had lower levels of CCL1, CCL2, CCL12, CXCL10, and CXCL12 and higher INFγ protein levels compared with the control tumor groups (Fig. 5A and B). On the basis of the known contribution of these cytokines to immune cell chemotaxis (29–32), we next examined immune cell infiltration into ovarian tumors grown in *WNT5A* knockouts and control cohorts. Interestingly, $Wnt5a^{KO}$, tamoxifen mice had a higher $CD8^{+/-}FOXP3^+$ ratio relative to controls (Fig. 6A and B), indicative of elevated cytotoxic T cells relative to regulatory T cells, a parameter that has been correlated with a better disease outcome in patients with ovarian cancer (33). Furthermore, $Wnt5a^{KO}$, tamoxifen mice had increased M1 macrophages and decreased infiltration of M2 macrophages (Fig.6C–F). A higher M1/M2 macrophage ratio has been previously correlated with better antitumor immunity and enhanced survival rates in patients with ovarian cancer (34, 35). Collectively, these data support a prometastatic role for host Wnt5a through potentiation of aggressive ovarian cancer cellular phenotypes and modulation of the host peritoneal immune landscape to an immunosuppressive environment.

## The Src family kinase Fgr is a key downstream effector of Wnt5a

In light of our data showing that Wnt5a induces prometastatic ovarian cancer cell behaviors, a phosphokinase array was used as an unbiased screen for activation of a panel of kinases in Wnt5a-treated cells. Although altered phosphorylation of many kinases was observed (both

enhanced and decreased; Fig. 7A), the Src family kinase Fgr exhibited the largest fold change in activation in response to Wnt5a (~18-fold) in both OVCAR5 and OVCAR8 cells (Fig. 7A and B). Phosphorylation of Fgr kinase (on Y412) was confirmed by immunoblotting and was detected as early as 15 minutes following Wnt5a addition (Fig. 7C). In OVCAR8 cells, phosphorylation was sustained for up to 6 hours. To assess the role of Wnt5a-induced Fgr phosphorylation in regulation of ovarian cancer cell behavior, we evaluated TL02–59, a potent, selective Fgr kinase inhibitor (Supplementary Fig. S4A). Inhibition of Fgr activity blocked Wnt5a-induced adhesion and motility in both OVCAR5 and OVCAR8 cells (Supplementary Fig. S4B–S4D; Fig. 7D–F), supporting a role for Fgr kinase activity in ovarian cancer metastatic progression. Moreover, IHC analysis of a human ovarian cancer tissue microarray ($n = 51$) containing late-stage (III, IV) tumors showed that 63% of specimens stained positively for phospho-Fgr (Y412; Supplementary Fig. S5). Given the lack of available antibodies directed against murine phospho-Fgr, tissues from the allograft study could not be evaluated for altered phosphokinase staining in *WNT5A* conditional knockouts. Collectively, these data highlight Fgr kinase as a downstream effector of Wnt5a signaling in ovarian cancer progression.

## Discussion

Because the high degree of genetic heterogeneity observed in ovarian tumors makes it difficult to identify a single clinically actionable genetic alteration, investigating the contribution of host microenvironmental factors to ovarian cancer progression and metastasis represents an alternative strategy for discovery of novel targets for therapeutic intervention. Herein, we show that peritoneally disseminated ovarian cancer cells encounter high Wnt5a levels contributed by host MC and adipocytes in the peritoneal microenvironment. Wnt5a induces aggressive and prometastatic cell behavior, activates the Src family kinase Fgr to accelerate peritoneal seeding, and potentiates an immunosuppressive immune landscape in ovarian tumors.

Previous studies have shown a strong link between Wnt5a and inflammation and a positive correlation between Wnt5a expression and the presence of immune cells in tumor tissues (8, 36). Wnt5a induces inflammatory cytokine secretion, leading to the recruitment of immune cells that augment cancer-associated inflammation (8). Although we cannot formally rule out potential cell-intrinsic effects of *WNT5A* depletion, particularly in macrophages, our results support these findings and show altered cytokine and chemokine secretion in peritoneal lavage from tumor-bearing control mice relative to *WNT5A* conditional knockouts with corresponding changes in macrophage polarization and T-cell phenotypes. Specifically, *WNT5A* knockout mice have low expression of CCL1, CCL2, CCL12, CXCL10, and CXCL12 in peritoneal lavage fluids. Previous studies demonstrated that these cytokines are expressed in both tumor and stromal cells and correlate with T regulatory cell and tumor-associated macrophage infiltration, metastatic homing of tumor cells, and poor prognosis (37–39). This is consistent with our data showing higher CD8/Treg and M1/M2 macrophage ratios in *WNT5A* knockout mice, and in women with ovarian cancer, these prognostic factors correlate with enhanced survival (33–35). In contrast, *WNT5A* knockout mice have upregulated expression of INF$\gamma$. Although several *in vivo* and *in vitro* preclinical studies show an antitumor effect of INF$\gamma$ in ovarian cancer (40–42), therapeutic trials using

INFγ have inconsistent outcomes (43). Nevertheless, several trials that incorporate INFγ in combination therapy regimens are ongoing in women with ovarian, fallopian tube, and primary peritoneal cancer, including studies to assess the efficacy of combined IFNγ with immune checkpoint inhibitors (33–35).

A large body of evidence links Src family kinases, particularly Src, with aggressive behavior in cancers including ovarian cancer (44). However, although preclinical studies identified Src as a strong candidate for targeted therapeutic intervention in ovarian cancer, clinical trials using the Src inhibitors dasatinib and saracatinib as single agents or in combination with paclitaxel in women with platinum-resistant tumors were disappointing, as they failed to show increased progression-free or overall survival (45–47). Recently, an unbiased discovery-based approach to detect candidate genes and molecular pathways associated with platinum resistance in a cohort of 53 patients with ovarian cancer identified upregulation of *WNT5A* and its receptor *ROR2* in platinum-resistant tumors (12). In light of these clinical results, noteworthy is a report showing that silencing of Src in ovarian cancer cells leads to compensatory upregulation of Fgr expression (48). Moreover, Fgr expression has been correlated with reduced infiltration of cytotoxic T lymphocytes and poor prognosis in colorectal cancer and additional studies demonstrate a role for Fgr in generation of the myeloid cell–mediated inflammatory response *in vivo* (49, 50). Together with our data showing that Wnt5a-induced Fgr activation and associated prometastatic ovarian cancer cell behaviors are blocked by the selective Fgr inhibitor TL02–59, further investigation of Fgr as a therapeutic target in metastatic ovarian cancer is warranted. In summary, our study establishes host-derived Wnt5a as a key factor regulating intraperitoneal dissemination of ovarian cancer and identifies Fgr as a novel molecular target for inhibition of metastatic progression.

## Supplementary Material

Refer to Web version on PubMed Central for supplementary material.

## Acknowledgments

This work was supported in part by research grants RO1 CA109545 (M.S. Stack), RO1 CA194697 (S. Zhang), and KO1 CA218305 (T.S. Hilliard) from the NIH, NCI; the Leo and Anne Albert Charitable Trust (M.S. Stack); and Walther Cancer Foundation Interdisciplinary Interface Training Program (M. Asem and E.I. Harper).

## References

1. Torre LA, Trabert B, DeSantis CE, Miller KD, Samimi G, Runowicz CD, et al. Ovarian cancer statistics, 2018. CA Cancer J Clin 2018;68:284–96. [PubMed: 29809280]
2. Mankoo PK, Shen R, Schultz N, Levine DA, Sander C. Time to recurrence and survival in serous ovarian tumors predicted from integrated genomic profiles. PLoS One 2011;6:e24709.
3. Hoogstraat M, de Pagter MS, Cirkel GA, van Roosmalen MJ, Harkins TT, Duran K, et al. Genomic and transcriptomic plasticity in treatment-naive ovarian cancer. Genome Res 2014;24:200–11. [PubMed: 24221193]
4. McBride DJ, Etemadmoghadam D, Cooke SL, Alsop K, George J, Butler A, et al. Tandem duplication of chromosomal segments is common in ovarian and breast cancer genomes. J Pathol 2012;227:446–55. [PubMed: 22514011]

5. Coffman LG, Burgos-Ojeda D, Wu R, Cho K, Bai S, Buckanovich RJ. New models of hematogenous ovarian cancer metastasis demonstrate preferential spread to the ovary and a requirement for the ovary for abdominal dissemination. Transl Res 2016;175:92–102. [PubMed: 27083386]
6. Pradeep S, Kim SW, Wu SY, Nishimura M, Chaluvally-Raghavan P, Miyake T, et al. Hematogenous metastasis of ovarian cancer: rethinking mode of spread. Cancer Cell 2014;26:77–91. [PubMed: 25026212]
7. Ahmed N, Stenvers KL. Getting to know ovarian cancer ascites: opportunities for targeted therapy-based translational research. Front Oncol 2013;3: 256. [PubMed: 24093089]
8. Asem MS. Wnt5a signaling in cancer. 2016;8:79.
9. Bitler BG, Nicodemus JP, Li H, Cai Q, Wu H, Hua X, et al. Wnt5a suppresses epithelial ovarian cancer by promoting cellular senescence. Cancer Res 2011;71: 6184–94. [PubMed: 21816908]
10. Park HW, Kim YC, Yu B, Moroishi T, Mo J-S, Plouffe SW, et al. Alternative Wnt signaling activates YAP/TAZ. Cell 2015;162:780–94. [PubMed: 26276632]
11. Ford CE, Punnia-Moorthy G, Henry CE, Llamosas E, Nixdorf S, Olivier J, et al. The non-canonical Wnt ligand, Wnt5a, is upregulated and associated with epithelial to mesenchymal transition in epithelial ovarian cancer. Gynecol Oncol 2014;134:338–45. [PubMed: 24924122]
12. Veskimäe K, Scaravilli M, Niininen W, Karvonen H, Jaatinen S, Nykter M, et al. Expression analysis of platinum sensitive and resistant epithelial ovarian cancer patient samples reveals new candidates for targeted therapies.Transl Oncol 2018; 11:1160–70. [PubMed: 30056367]
13. Roby KF, Taylor CC, Sweetwood JP, Cheng Y, Pace JL, Tawfik O, et al. Development of a syngeneic mouse model for events related to ovarian cancer. Carcinogenesis 2000;21:585–91. [PubMed: 10753190]
14. Liu Y, Metzinger MN, Lewellen KA, Cripps SN, Carey KD, Harper EI, et al. Obesity contributes to ovarian cancer metastatic success through increased lipogenesis, enhanced vascularity, and decreased infiltration of M1 macrophages. Cancer Res 2015;75:5046–57. [PubMed: 26573796]
15. Blum W, Pecze L, Felley-Bosco E, Worthmüller-Rodriguez J, Wu L, Vrugt B, et al. Establishment of immortalized murine mesothelial cells and a novel mesothelioma cell line. In Vitro Cell Dev Biol Anim 2015;51:714–21. [PubMed: 25877069]
16. Kenny HA, Dogan S, Zillhardt M, K Mitra A, Yamada SD, Krausz T, et al. Organotypic models of metastasis: A three-dimensional culture mimicking the human peritoneum and omentum for the study of the early steps of ovarian cancer metastasis. Cancer Treat Res 2009;149:335–51. [PubMed: 19763444]
17. Fuster JJ, Zuriaga MA, Ngo DT, Farb MG, Aprahamian T, Yamaguchi TP, et al. Noncanonical Wnt signaling promotes obesity-induced adipose tissue inflammation and metabolic dysfunction independent of adipose tissue expansion. Diabetes 2015;64:1235–48. [PubMed: 25352637]
18. Loughran EA, Leonard AK, Hilliard TS, Phan RC, Yemc MG, Harper E, et al. Aging Increases susceptibility to ovarian cancer metastasis in murine allograft models and alters immune composition of peritoneal adipose tissue. Neoplasia 2018;20:621–31. [PubMed: 29754071]
19. Sodek KL, Murphy KJ, Brown TJ, Ringuette MJ. Cell-cell and cell-matrix dynamics in intraperitoneal cancer metastasis. Cancer Metastasis Rev 2012; 31:397–414. [PubMed: 22527451]
20. Nagy JA. Peritoneal membrane morphology and function. Kidney Int Suppl 1996;56:S2–11. [PubMed: 8914047]
21. Lengyel E, Burdette JE, Kenny HA, Matei D, Pilrose J, Haluska P, et al. Epithelial ovarian cancer experimental models. Oncogene 2014;33:3619–33. [PubMed: 23934194]
22. Barbolina MV, Burkhalter RJ, Stack MS. Diverse mechanisms for activation of Wnt signalling in the ovarian tumour microenvironment. Biochem J 2011;437: 1–12. [PubMed: 21668411]
23. Naora H, Montell DJ. Ovarian cancer metastasis: integrating insights from disparate model organisms. Nat Rev Cancer 2005;5:355–66. [PubMed: 15864277]
24. Cátalan V, Gómez-Ambrosi J, Rodríguez A, Pérez-Hernández AI, Gurbindo J, Ramírez B, et al. Activation of noncanonical Wnt signaling through WNT5A in visceral adipose tissue of obese subjects is related to inflammation. J Clin Endocrinol Metab 2014;99:E1407–17. [PubMed: 24840810]

25. Jin Z, Zhao C, Han X, Han Y. Wnt5a promotes ewing sarcoma cell migration through upregulating CXCR4 expression. BMC Cancer 2012;12:480. [PubMed: 23075330]
26. Rauner M, Stein N, Winzer M, Goettsch C, Zwerina J, Schett G, et al. WNT5A is induced by inflammatory mediators in bone marrow stromal cells and regulates cytokine and chemokine production. J Bone Miner Res 2012;27:575–85. [PubMed: 22162112]
27. Ghosh MC, Collins GD, Vandanmagsar B, Patel K, Brill M, Carter A, et al. Activation of Wnt5A signaling is required for CXC chemokine ligand 12-mediated T-cell migration. Blood 2009;114:1366–73. [PubMed: 19520808]
28. Zhao C, Bu X, Wang W, Ma T, Ma H. GEC-derived SFRP5 inhibits Wnt5a-induced macrophage chemotaxis and activation. PLoS One 2014;9:e85058.
29. Hoelzinger DB, Smith SE, Mirza N, Dominguez AL, Manrique SZ, Lustgarten J. Blockade of CCL1 inhibits T regulatory cell suppressive function enhancing tumor immunity without affecting T effector responses. J Immunol 2010;184: 6833–42. [PubMed: 20483762]
30. Marazioti A, Kairi CA, Spella M, Giannou AD, Magkouta S, Giopanou I, et al. Beneficial impact of CCL2 and CCL12 neutralization on experimental malignant pleural effusion. PLoS One 2013;8:e71207.
31. Liu M, Guo S, Stiles JK. The emerging role of CXCL10 in cancer (Review). Oncol Lett 2011;2:583–589. [PubMed: 22848232]
32. Zaidi MR, Merlino G. The two faces of interferon-gamma in cancer. Clin Cancer Res 2011;17:6118–24. [PubMed: 21705455]
33. Preston CC, Maurer MJ, Oberg AL, Visscher DW, Kalli KR, Hartmann LC, et al. The ratios of CD8+ T cells to CD4+CD25+ FOXP3+ and FOXP3- T cells correlate with poor clinical outcome in human serous ovarian cancer. PLoS One 2013;8:e80063.
34. Gupta V, Yull F, Khabele D. Bipolar tumor-associated macrophages in ovarian cancer as targets for therapy. Cancers 2018;10.pii:E366.
35. Zhang M, He Y, Sun X, Li Q, Wang W, Zhao A, et al. A high M1/M2 ratio of tumor-associated macrophages is associated with extended survival in ovarian cancer patients. J Ovarian Rese 2014;7:19.
36. Pashirzad M, Shafiee M, Rahmani F, Behnam-Rassouli R, Hoseinkhani F, Ryzhikov M, et al. Role of Wnt5a in the pathogenesis of inflammatory diseases. J Cell Physiol 2017;232:1611–6. [PubMed: 27859213]
37. Ben-Baruch A. Inflammation-associated immune suppression in cancer: the roles played by cytokines, chemokines and additional mediators. Semin Cancer Biol 2006;16:38–52. [PubMed: 16139507]
38. Fujimoto H, Sangai T, Ishii G, Ikehara A, Nagashima T, Miyazaki M, et al. Stromal MCP-1 in mammary tumors induces tumor-associated macrophage infiltration and contributes to tumor progression. Int J Cancer 2009;125:1276–84. [PubMed: 19479998]
39. Kuehnemuth B, Piseddu I, Wiedemann GM, Lauseker M, Kuhn C, Hofmann S, et al. CCL1 is a major regulatory T cell attracting factor in human breast cancer. BMC Cancer 2018;18:1278. [PubMed: 30572845]
40. Green DS, Husain SR, Johnson CL, Sato Y, Han J, Joshi B, et al. Combination immunotherapy with IL-4 Pseudomonas exotoxin and IFN-alpha and IFN-gamma mediate antitumor effects in vitro and in a mouse model of human ovarian cancer. Immunotherapy 2019;11:483–96. [PubMed: 30860437]
41. Wall L, Burke F, Barton C, Smyth J, Balkwill F. IFN-gamma induces apoptosis in ovarian cancer cells in vivo and in vitro. Clin Cancer Res 2003;9:2487–96. [PubMed: 12855622]
42. Green DS, Nunes AT, Annunziata CM, Zoon KC. Monocyte and interferon based therapy for the treatment of ovarian cancer. Cytokine Growth Factor Rev 2016;29:109–15. [PubMed: 27026228]
43. Mojic M, Takeda K, Hayakawa Y. The dark side of IFN-gamma: its role in promoting cancer immunoevasion. Int J Mol Sci 2017;19:pii:E89.
44. Sen B, Johnson FM. Regulation of SRC family kinases in human cancers. J Signal Transduct 2011;2011:865819.
45. Banerjee S, Kaye SB. New strategies in the treatment of ovarian cancer: current clinical perspectives and future potential. Clin Cancer Res 2013;19: 961–8. [PubMed: 23307860]

46. Schilder RJ, Brady WE, Lankes HA, Fiorica JV, Shahin MS, Zhou XC, et al. Phase II evaluation of dasatinib in the treatment of recurrent or persistent epithelial ovarian or primary peritoneal carcinoma: a Gynecologic Oncology Group study. Gynecol Oncol 2012;127:70–4. [PubMed: 22710075]

47. McNeish IA, Ledermann JA, Webber L, James L, Kaye SB, Hall M, et al. A randomised, placebo-controlled trial of weekly paclitaxel and saracatinib (AZD0530) in platinum-resistant ovarian, fallopian tube or primary peritoneal cancerdagger. Ann Oncol 2014;25:1988–95. [PubMed: 25070546]

48. Kim H-S, Han HD, Armaiz-Pena GN, Stone RL, Nam EJ, Lee J-W, et al. Functional roles of Src and Fgr in ovarian carcinoma. Clin Cancer Res 2011; 17:1713–21. [PubMed: 21300758]

49. Kovács M, Németh T, Jakus Z, Sitaru C, Simon E, Futosi K, et al. The Src family kinases Hck, Fgr, and Lyn are critical for the generation of the in vivo inflammatory environment without a direct role in leukocyte recruitment. J Exp Med 2014;211:1993–2011. [PubMed: 25225462]

50. Mazzi P, Caveggion E, Lapinet-Vera JA, Lowell CA, Berton G. The Src-family kinases Hck and Fgr regulate early lipopolysaccharide-induced myeloid cell recruitment into the lung and their ability to secrete chemokines. J Immunol 2015;195:2383–95. [PubMed: 26232427]

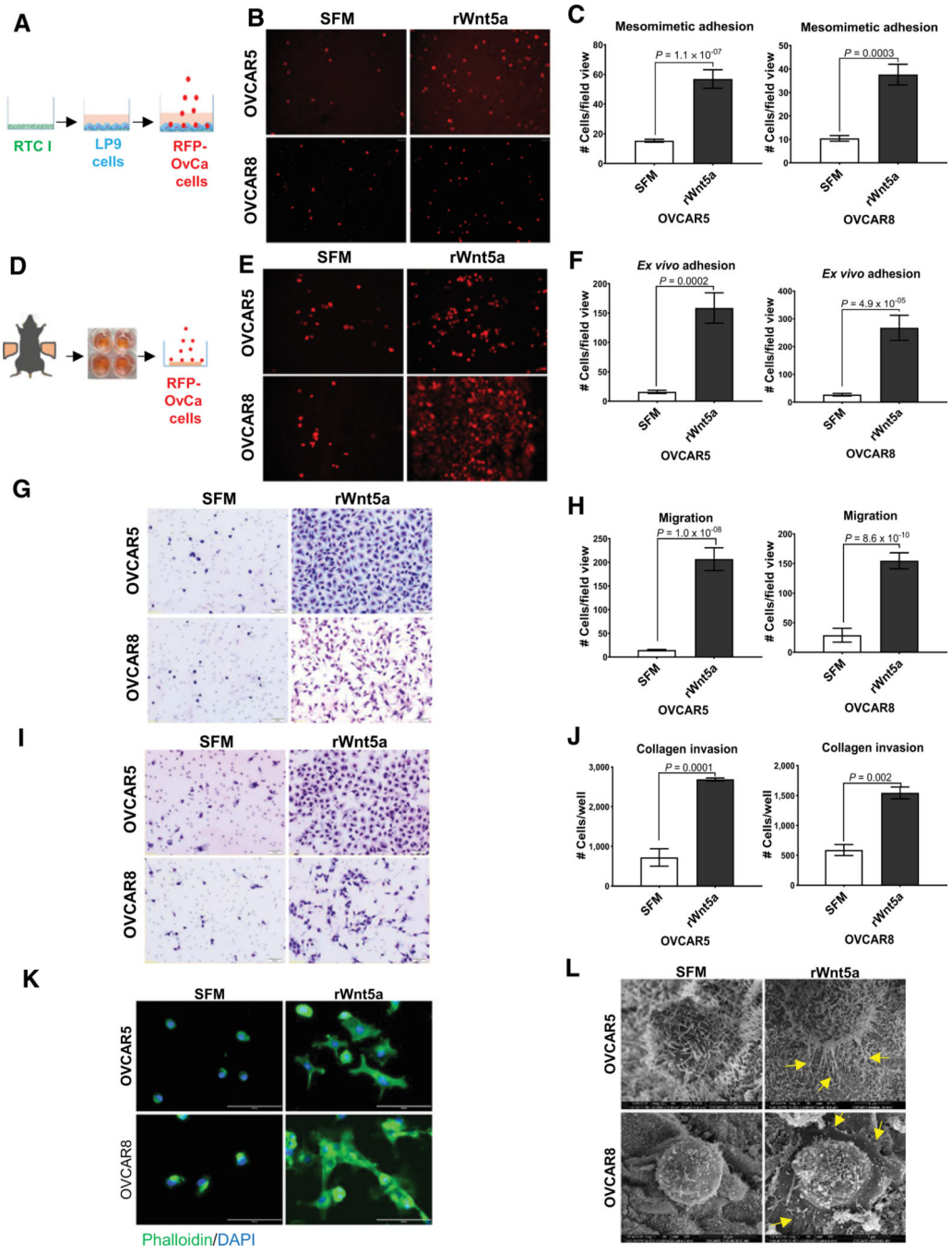


**Figure 1.**

Wnt5a induces prometastatic ovarian cancer cell phenotypes. **A,** Diagram of mesomimetic culture comprised of three-dimensional type I collagen (RTC I) gels overlaid with LP9 human peritoneal MC (20). **B,** RFP-tagged OVCAR5 and OVCAR8 cells were treated with SFM or recombinant Wnt5a protein (rWnt5a; 0.4 μg/mL, 24 hours) as indicated. Cells from each treatment condition ($5 \times 10^4$) were incubated with mesomimetic cultures for 20 minutes or 1 hour, respectively, prior to washing and imaging. **C,** Quantification of adherent cells. **D,** Diagram of murine *ex vivo* peritoneal explant culture. Explants were pinned

mesothelium-up on optically clear silastic resin. **E,** RFP-tagged OVCAR5 and OVCAR8 cells were treated with SFM or rWnt5a (0.4 μg/mL, 24 hours) as indicated prior to incubation with murine peritoneal explants in an *ex vivo* adhesion assay for 30 or 90 minutes, respectively, prior to washing and imaging. **F,** Quantification of adherent cells. Images of adherent cells were obtained using Echo Revolve fluorescent microscope at ×20 magnification. **G,** OVCAR5 and OVCAR8 cells were added to transwell migration chambers containing SFM or rWnt5a (0.4 μg/mL) and incubated for 12 and 18 hours, respectively. Migrated cells were fixed and stained with Diff-Quik Kit. **H,** Quantification of migrated cells. **I,** OVCAR5 and OVCAR8 cells were added to transwell invasion chambers containing type I collagen (100 μL of 200 μg/mL) and SFM or rWnt5a (0.4 μg/mL, 24 hours). Invaded cells were fixed and stained with Diff-Quik Kit. **J,** Quantification of invaded cells. Images of migrated and invaded cells were obtained using Olympus BH-42 microscope. Scale bar, 20 μm. All experiments in **A–J** were performed as triplicates, with three independent biological replicates per cell line. All results are presented as mean ± SEM and *P* values were calculated using a Student two-tailed *t* test. $P < 0.05$ is statistically significant. **K,** OVCAR5 and OVCAR8 cells were serum-starved overnight, then resuspended in SFM or rWnt5a (0.4 μg/mL) and cultured atop collagen I-coated coverslips for 24 hours. Cells were fixed with 4% PFA buffer and stained with Phalloidin 488 and DAPI. Cells were imaged with Leica DM5500 fluorescence microscope at ×25 magnification. Scale bar, 100 μm. **L,** OVCAR5 and OVCAR8 cells were incubated in SFM or rWnt5a (0.4 μg/mL) for 24 hours. Cells were added to murine peritoneal explants for 30 and 90 minutes, respectively. The peritoneal explants were fixed and processed for imaging by FEI-Magellan 400 Field Emission scanning electron microscope. Scale bar, 5, 10 μm.

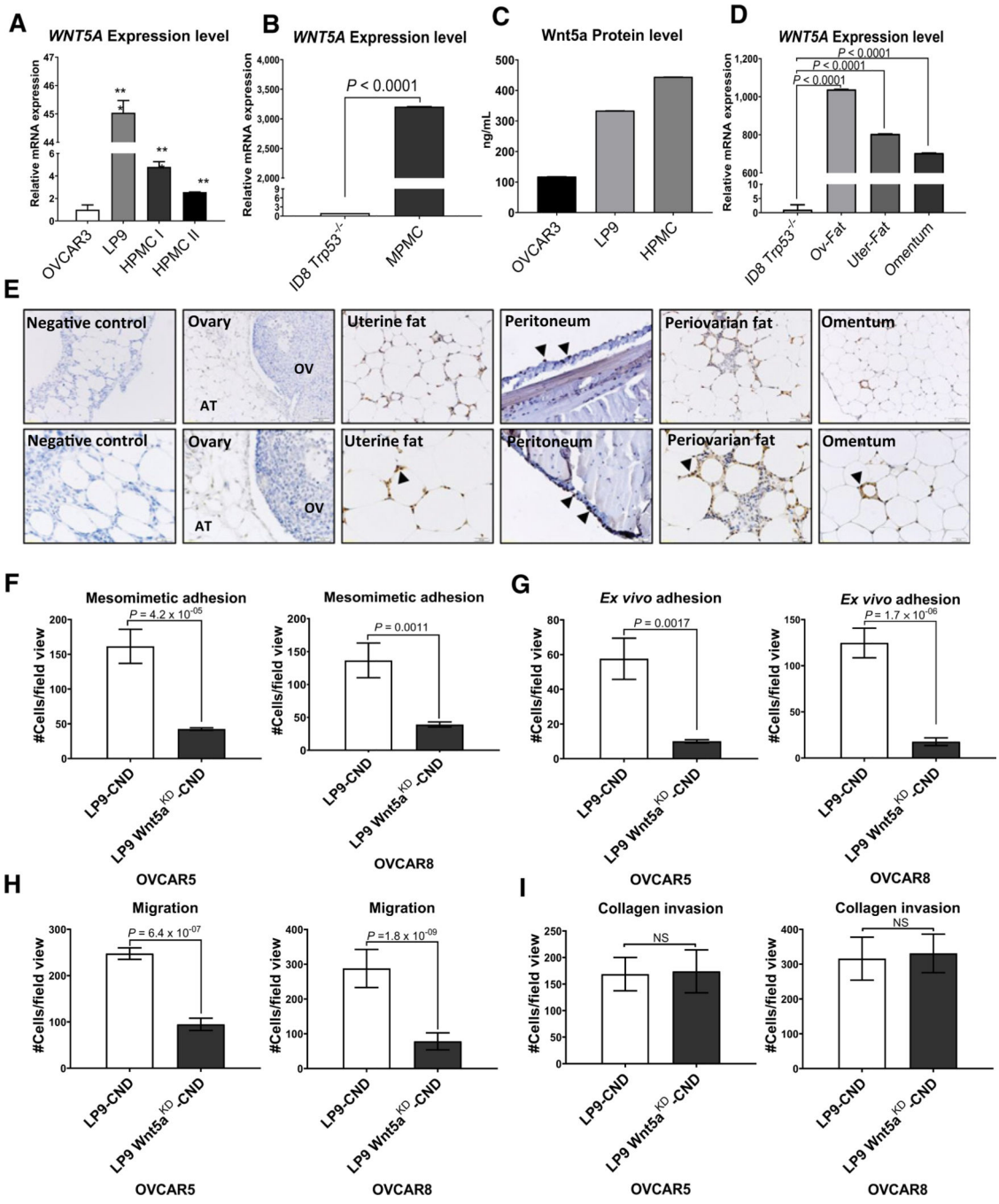


**Figure 2.**

Wnt5a derived from peritoneal mesothelial cells alters ovarian cancer cell behavior. **A–D,** Relative expression of *WNT5A* by qRT-PCR. **A,** Comparison of expression levels between the human ovarian cancer cell line OVCAR3, the human peritoneal mesothelial cell line LP9, and primary human peritoneal mesothelial cells from two different donors (HPMC I and HPMC II). **B,** Comparison of expression levels between the murine ovarian cancer cell line ID8-Trp53$^{-/-}$ and primary murine mesothelial cells (MPMC). **C,** Quantitation of Wnt5a protein level. The concentration of Wnt5a was measured in serum-free conditioned media

from OVCAR3, LP9, and HPMC cells using ELISA according to the manufacturer's specifications. **D,** Comparison of expression between the murine ovarian cancer cell line ID8-Trp53$^{-/-}$ and murine visceral adipose obtained from periovarian fat (Ov-fat), periuterine fat (uter-fat), or omentum. All experiments in **A–D** were performed using $n = 3$ independent biological replicates per experiment. Results are presented as mean ± SEM, and statistical significance was calculated using a Student two-tailed *t* test. $P < 0.05$ is statistically significant. **E,** IHC analysis of Wnt5a in murine ovarian tissue, uterine fat, peritoneum, periovarian fat, and omentum, as indicated. Tissues were incubated with anti-Wnt5a (1:200 dilution), followed by a peroxidase-conjugated anti–rabbit-IgG and peroxidase detection using DAB as described in Materials and Methods. Images were acquired with Olympus BH-42 microscope. Scale bar, 50 and 20 μm. Arrowheads, example areas of positive staining. **F,** Quantification of ovarian cancer cell adhesion to mesomimetic cultures. RFP-tagged OVCAR5 and OVCAR8 cells were serum-starved overnight, treated with conditioned medium from control human peritoneal MC (LP9-CND) or from LP9 cells in which *WNT5A* is silenced (LP9-Wnt5a$^{KD}$-CND) for 24 hours, then allowed to adhere to a mesomimetic culture 20 minutes and 1 hour, respectively. **G,** Quantification of ovarian cancer cell adhesion to murine peritoneal explants. RFP-tagged OVCAR5 and OVCAR8 cells were treated with either LP9-CND or LP9-Wnt5a$^{KD}$-CND for 24 hours prior to incubation with murine peritoneal explants in an *ex vivo* adhesion assay for 30 and 90 minutes, respectively. **H,** Analysis of migration. OVCAR5 and OVCAR8 cells were serum-starved overnight, then, cells were added to transwell migration chambers containing LP9-CND or LP9-Wnt5a$^{KD}$-CND and incubated for 12 and 18 hours, respectively. Migrated cells were fixed and stained with Diff-Quik Kit and quantified using ImageJ. **I,** Analysis of invasion. OVCAR5 and OVCAR8 cells were serum-starved overnight, then, cells were added to transwell invasion chambers containing type I collagen gels (100 μL of 200 μg/mL) with LP9-CND or LP9-Wnt5a$^{KD}$-CND and incubated for 24 hours. Invaded cells were fixed and stained with Diff-Quik Kit and quantified using ImageJ. All experiments were done in triplicate, with three independent biological replicates per each cell line. All results are presented as mean ± SEM and *P*-values were calculated using a Student two-tailed *t* test. $P < 0.05$ is statistically significant. NS, nonsignificant; *, $P < 0.05$; **, $P < 0.01$.

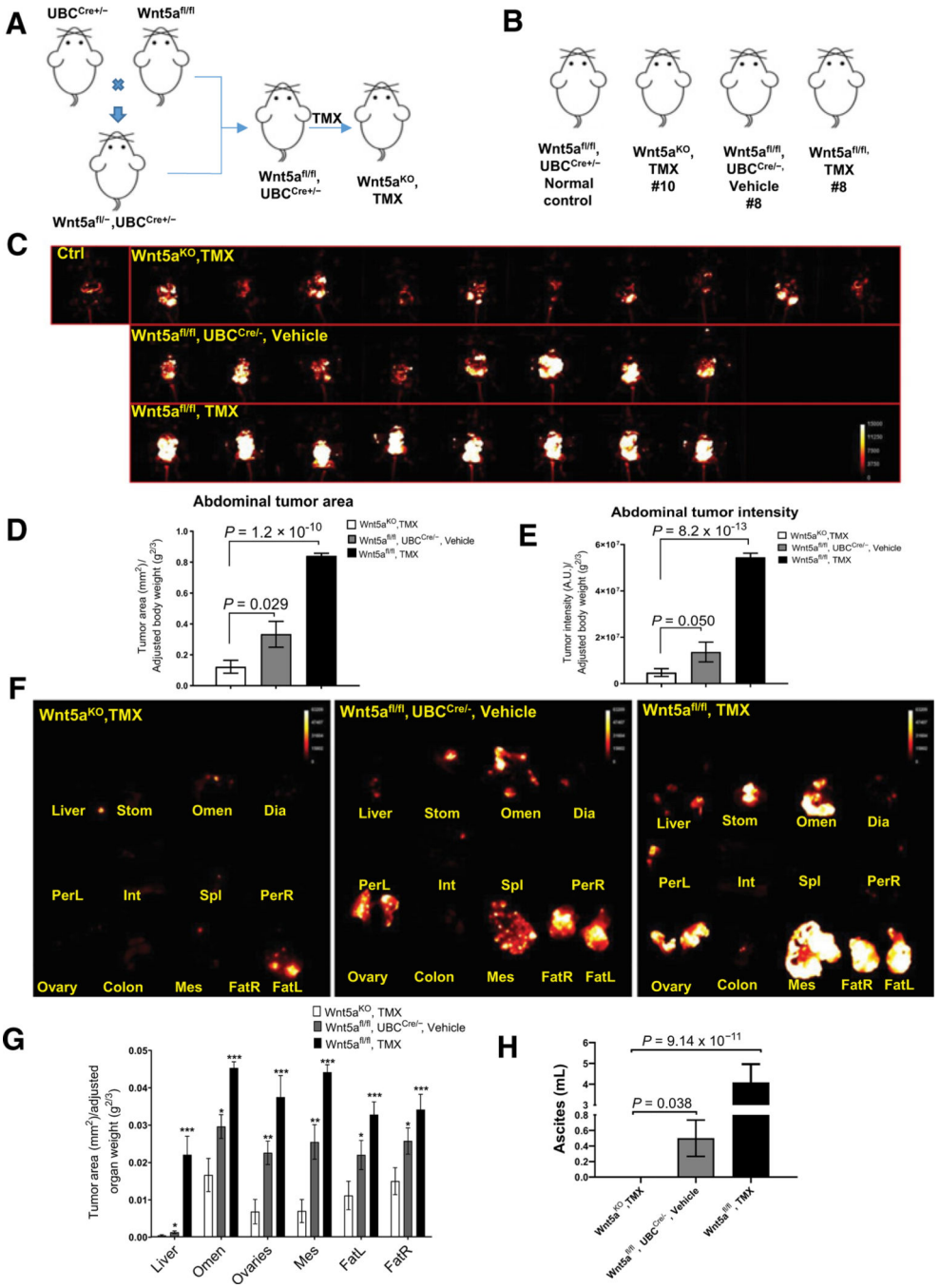


**Figure 3.**

Conditional silencing of host *WNT5A* reduces overall peritoneal metastatic burden. **A,** Overview of breeding strategy and tamoxifen (TMX) treatment to generate *WNT5A* knockout mice. **B,** Summary of murine cohorts used in the allograft tumor study. **C,** Mice were injected intraperitoneally with $5 \times 10^6$ RFP-tagged ID8-Trp53$^{-/-}$ syngeneic murine ovarian cancer cells. Beginning at 3 weeks postinjection, tumor burden *in situ* was longitudinally imaged weekly using a Bruker Xtreme In Vivo Imaging system. Mice were sacrificed at 5 weeks postinjection and each abdominal cavity was exposed and imaged

using the Bruker Xtreme In Vivo Imaging system. **E,** Quantification of abdominal tumor burden area by dividing the tumor area by the scale-adjusted body weight of each mouse. **E,** Abdominal tumor intensity was calculated by dividing the tumor intensity by the scale-adjusted body weight of each mouse. Quantification was performed using ImageJ. All results are presented as means ± SEM and *P* values were calculated using a Student two-tailed *t* test. $P < 0.05$ is statistically significant. **F,** Representative organ-specific tumor burden images for each cohort. Individual organs were dissected and imaged *ex vivo* using the Bruker Xtreme In Vivo Imaging system. **G,** Quantification of organ-specific tumor burden. The "organ area fraction" was quantified by dividing the tumor area by the adjusted organ weight for all mice in each cohort. **H,** All mice were subjected to peritoneal lavage with 2 mL of PBS, then, ascites/PBS fluid was collected. Ascites volume was calculated by subtracting 2 from the total volume. All results are presented as mean ± SEM and *P* values were calculated using a Student two-tailed *t* test. *, $P < 0.05$; **, $P < 0.01$; ***, $P < 0.001$, with $P < 0.05$ being statistically significant.

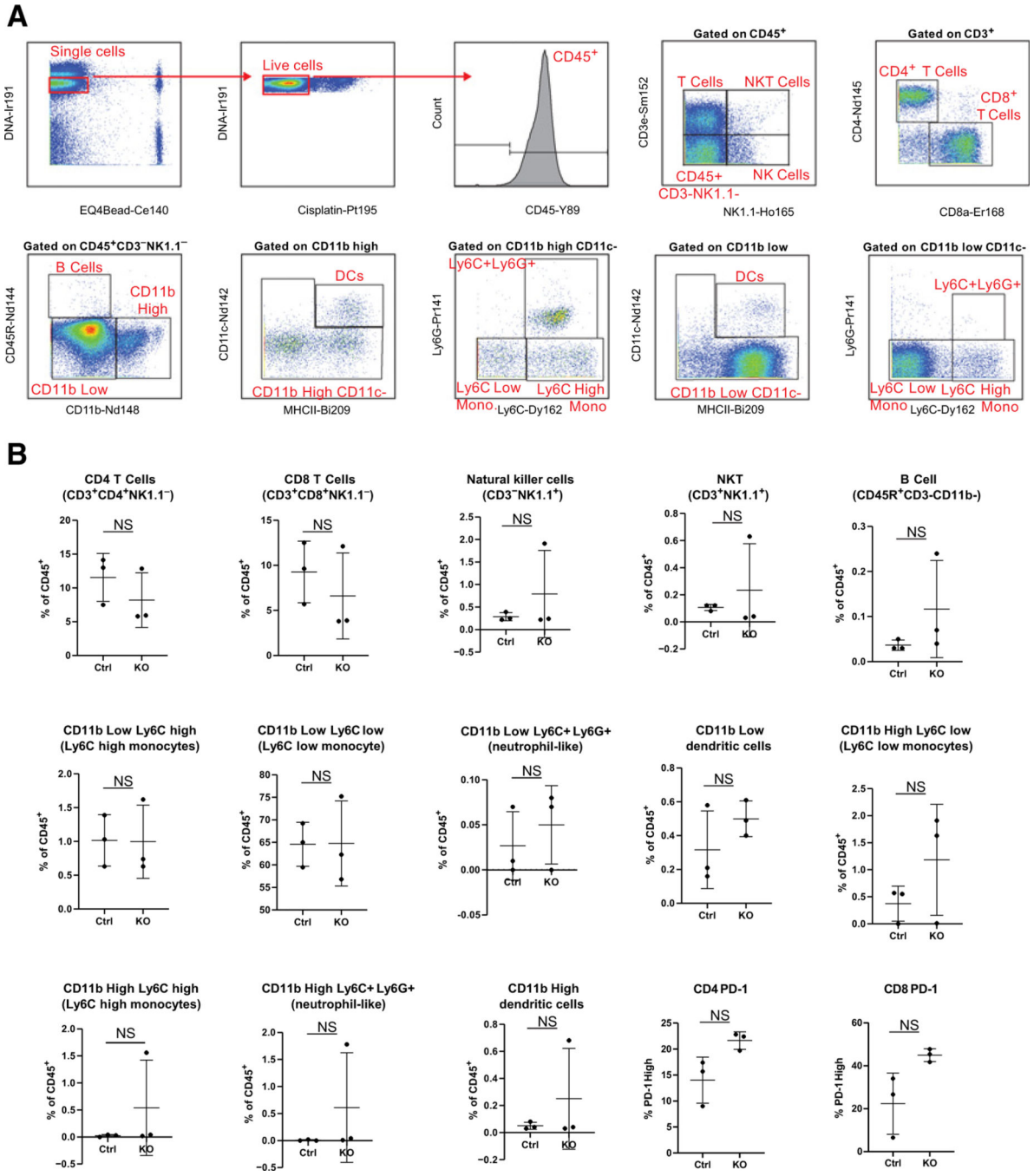


**Figure 4.**

CyTOF analysis of immune profiles in peritoneal lavage. Peritoneal lavage was collected from tumor-free Wnt5a$^{KO}$ and control mice ($n$ = 3/genotype) as described in Materials and Methods and labeled with metal-conjugated antibodies for mass cytometry analysis as described previously. **A,** Gating strategy for CyTOF data. **B,** Frequencies of indicated immune populations of all CD45$^{+}$ immune cells and PD-1 expression in indicated T-cell subsets in control (Ctrl) versus Wnt5a$^{KO}$ (KO) hosts. NS, data do not reach statistical significance ($P > 0.05$).

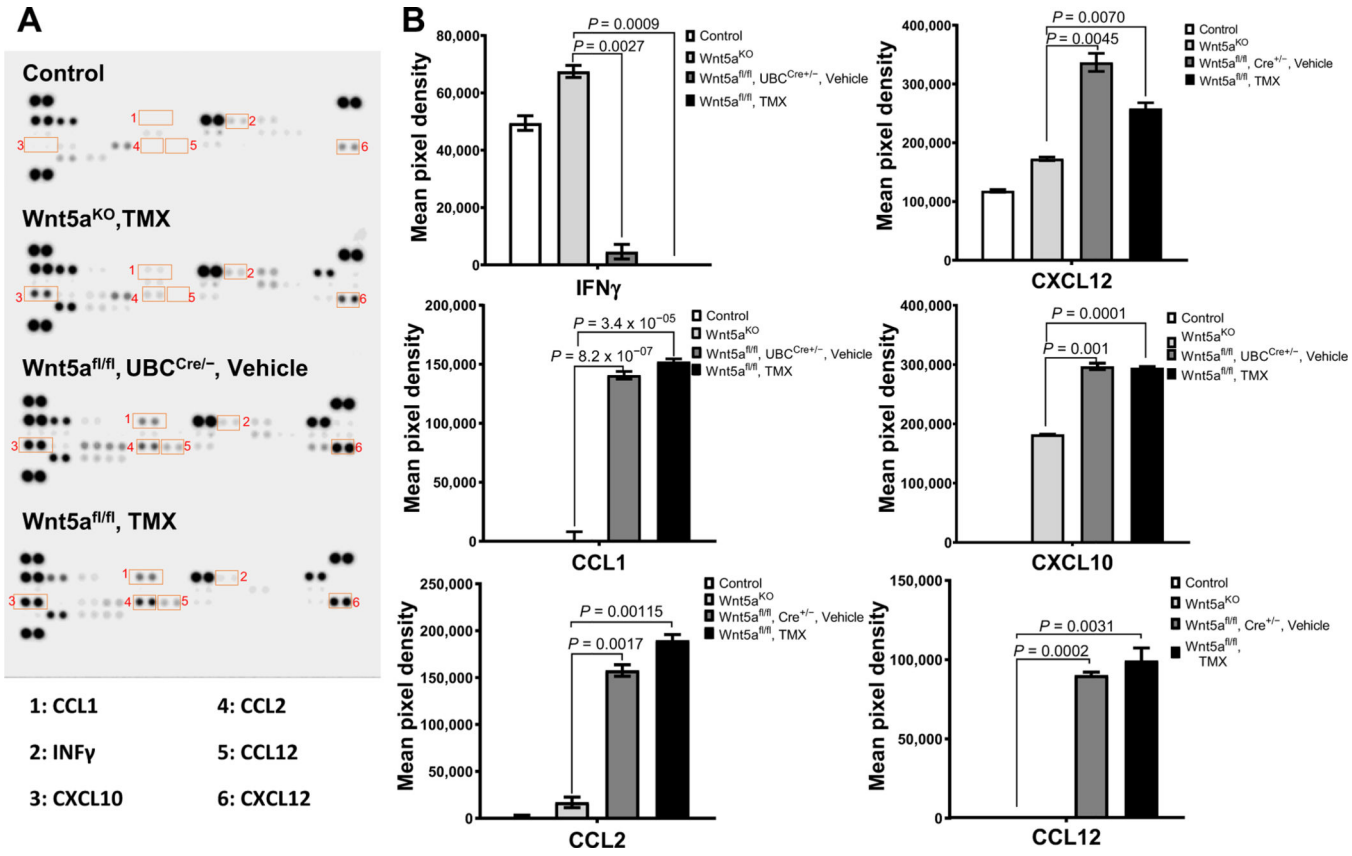


**Figure 5.**

Tumor-bearing *WNT5A* knockout mice have altered peritoneal cytokine profiles. **A,** Peritoneal lavage obtained from mice with conditional *WNT5A* knockout or controls was analyzed using the murine Proteome Profiler Cytokine Array according to the manufacturer's specifications. Spots showing differential expression are boxed.**B,** Each cytokine has duplicate spots on the blot and each spot intensity was quantified by measuring pixel density using ImageJ following the manufacturer's protocol. All results are presented as mean ± SEM.

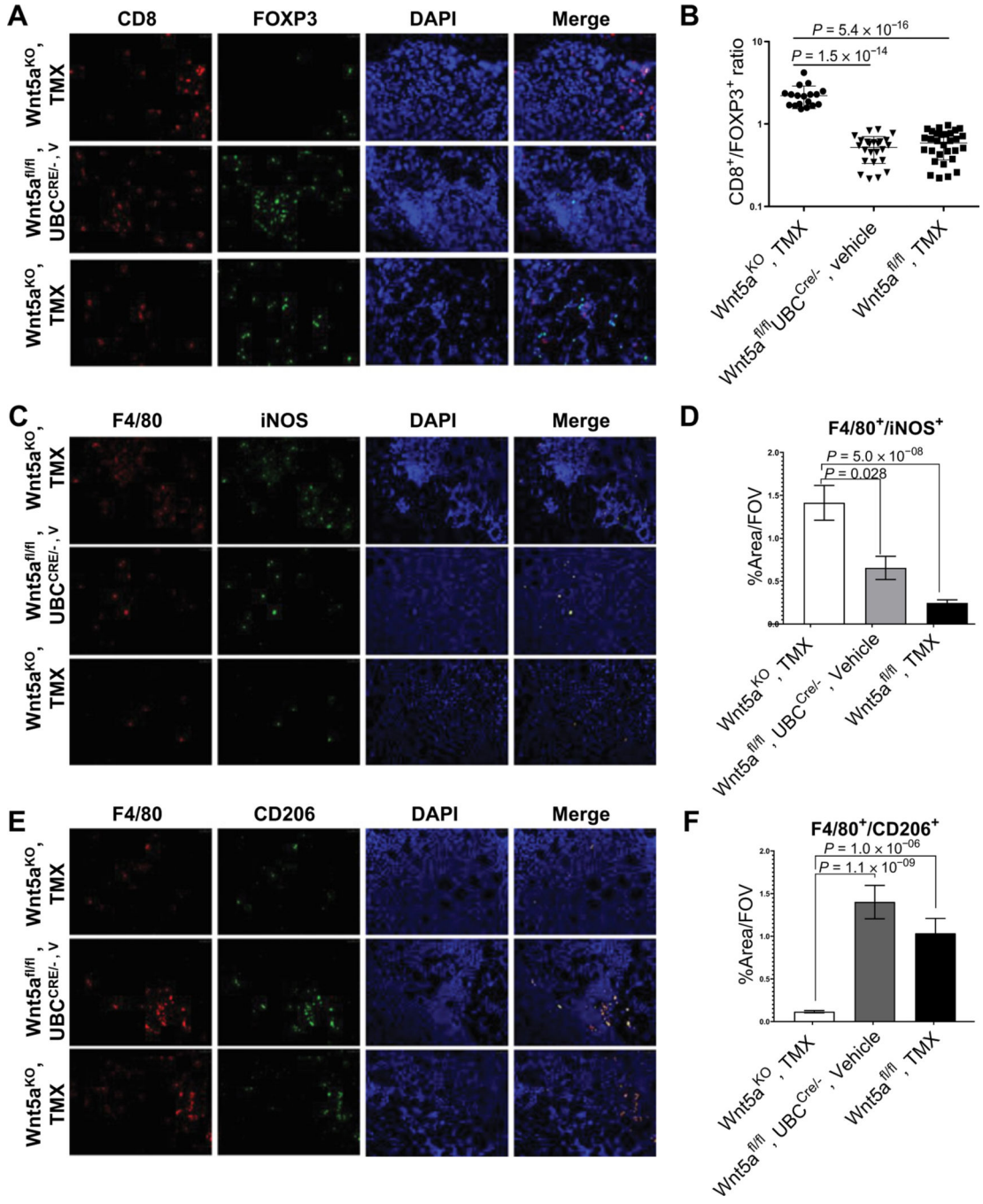


**Figure 6.**

Silencing of host *WNT5A* alters the immune landscape of peritoneal metastases. **A,** Immunofluorescence staining of infiltrating FOXP3$^+$ T cells (red) and CD8$^+$ T cells (green) in peritoneal metastases at magnification ×20. **B,** The ratio of average of CD8$^+$ and FOXP3$^+$ cell counts for three mice from each cohort was used for statistical analysis. Cell counting was done manually in ImageJ. **C,** Immunofluorescence staining of infiltrating F4/80$^+$ (red) iNOS$^+$ (green) M1 macrophages in peritoneal metastases. **E,** Immunofluorescence staining of infiltrating F4/80$^+$ (red) CD206$^+$ (green) M2 macrophages in peritoneal metastases. **D–F,**

For macrophage quantification, 10 independent areas with the most abundant macrophages per mouse were selected and imaged with 20 objective lens and area percentage covered by $F4/80^+$ $iNOS^+$ or $F4/80^+$ $CD206^+$ cells was calculated per each image using ImageJ. A representative image is shown. Imaging was done with Leica DM5500 fluorescence microscope. All results are presented as means ± SEM, and *P* values were calculated using a Student two-tailed *t* test. $P < 0.05$ is statistically significant.

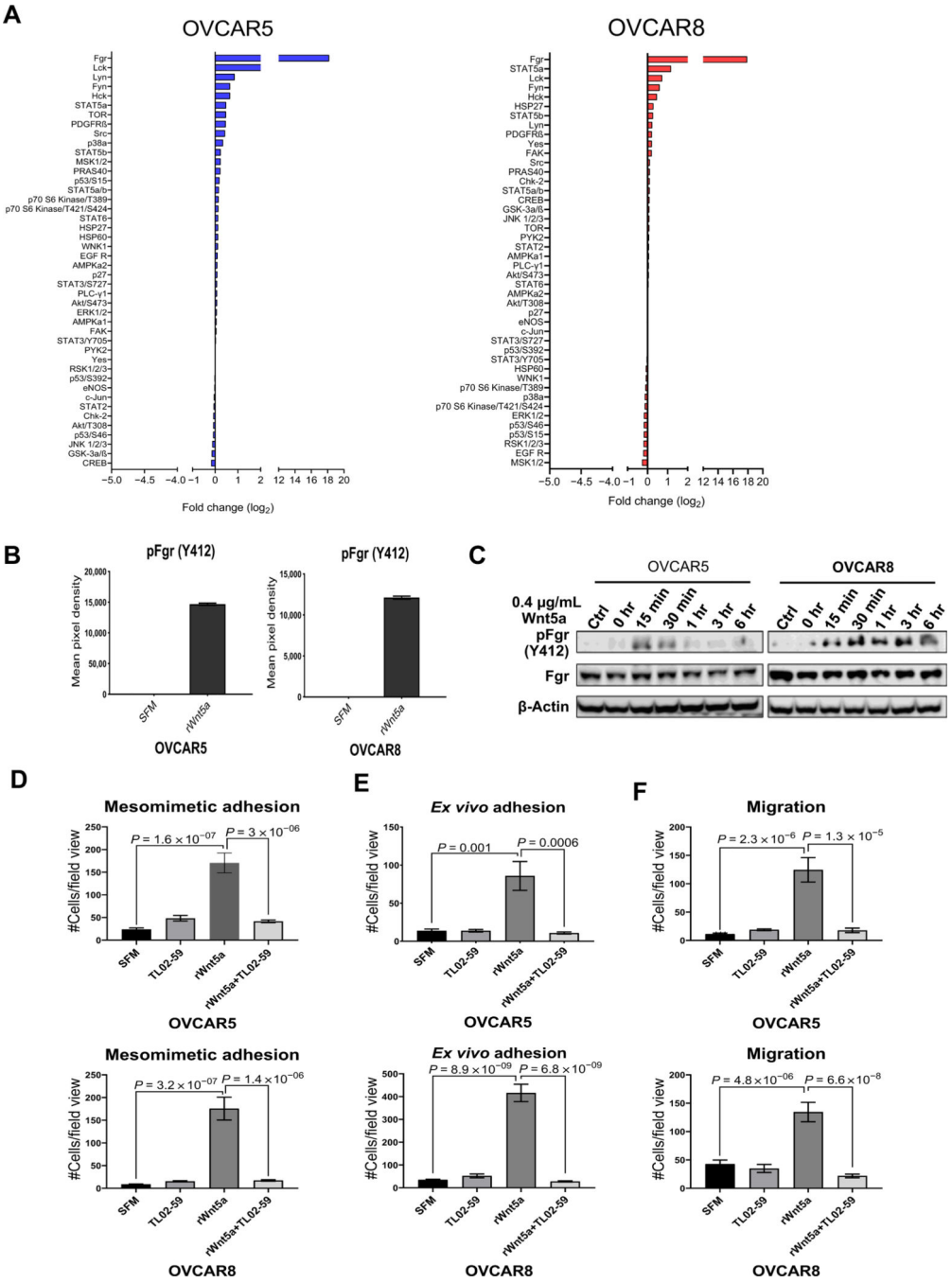


**Figure 7.**

Identification of Fgr as a downstream mediator of Wnt5a prometastatic cellular behavior. **A,** OVCAR5 and OVCAR8 cells were treated with SFM or rWnt5a protein (0.4 µg/mL, 24 hours) prior to lysis. Lysates were analyzed using the Proteome Profiler Human Phospho-Kinase Array according to the manufacturer's specifications. $Log_2$-fold change of phosphorylated proteins in the phosphokinase array is shown. **B,** Quantification of Fgr (Y412) phosphorylation by measuring pixel density for duplicate spots on the phospho-array blot using ImageJ. Data are presented as mean ± SEM. **C,** Validation of Fgr expression and

phosphorylation. OVCAR5 and OVCAR8 cells were serum-starved for 2 hours then incubated with the Fgr inhibitor TL02–59 (0.01 μmol/L) for 2.5 hours. After washing, cells in SFM were incubated with rWnt5a protein (0.4 μg/mL) for the time points indicated. Ctrl, cells without rWnt5a treatment. Lysates were electrophoresed on SDS-polyacrylamide gels and immunoblotted with the antibodies noted. One representative blot from three independent biological replicates is shown. **D** and **E,** RFP-tagged OVCAR5 and OVCAR8 cells were treated with SFM, rWnt5a (0.4 mg/mL), rWnt5a (0.4 μg/mL), and the specific Fgr kinase inhibitor TL02–59 (1 μmol/L) or TL02–59 (1 μmol/L) for 24 hours, as indicated, prior to incubation with mesomimetic culture for 20 minutes or 1 hour (**D**), respectively, or with murine peritoneal explants in an *ex vivo* adhesion assay for 30 or 90 minutes (**E**), respectively. Quantification of adherent cells is shown for each condition. **F,** OVCAR5 and OVCAR8 cells were added to transwell migration chambers containing SFM, rWnt5a (0.4 μg/mL), rWnt5a (0.4 μg/mL), and TL02–59 (1 μmol/L), or TL02–59 (1 μmol/L) and incubated for 12 and 18 hours, respectively. Quantification of migrated cells in each condition.